PAPER

Check for updates

Facile synthesis of a luminescent carbon material from yogurt for the efficient photocatalytic degradation of methylene blue

Muhammad Ali Bhatti,[a] Aneela Tahira,[b] Aqeel Ahmed Shah,[e] Umair Aftab, [ID][c] Brigitte Vigolo, [ID][d] Amira R. Khattab, [ID][i] Ayman Nafady,[g] Imran Ali Halepoto,[h] Matteo Tonezzer [ID][f] and Zafar Hussain Ibupoto [ID]*[b]

The present study is focused on yogurt as a simple, inexpensive, abundant, and green source for the preparation of luminescent carbon material for enhancing the photodegradation of methylene blue (MB). It introduces an ecological and sustainable approach for the large-scale production of carbon material using the direct thermal annealing of yogurt in a muffle furnace. The size of the as-prepared carbon material is about 200–300 nm, with average particle size distribution of 355 nm. The material exhibits clear luminescence under illumination with ultraviolet light. The synthesized carbon material shows an outstanding degradation functionality of MB under the irradiation of ultraviolet (UV) light in aqueous media. Various dye degradation parameters such as initial dye concentration, catalyst dose, pH of dye solution, and scavenger effects have been investigated. The optimum MB concentration was found to be 2.3×10^{-5} M with a degradation efficiency of 94.8%. The degradation was highly enhanced at pH 11 with a degradation efficiency of 98.11%. The degradation of MB under highly alkaline conditions was mainly governed by the high amount of hydroxyl radicals. Furthermore, the scavenger study confirmed that the hydroxyl radicals were mainly involved in the degradation process. The degradation kinetics of MB followed first order kinetics with large values of rate constant. The reusability was also studied to ensure the stability of the as-prepared carbon material during the degradation of MB. The preparation of carbon materials with efficient photosensitivity for the degradation of organic dyes from yogurt shows a green and innovative methodology. Therefore, it can be of great interest for future studies related to energy and environmental applications.

1. Introduction

Recently, the synthesis of nanostructured materials based on biomass assistance has received significant attention by researchers around the world. In this preparation, it is mainly dependent on biomolecules that chemically react under mild reaction conditions in the absence of toxic chemicals.[1–3] In the

[a]Institute of Environmental Sciences, University of Sindh, Jamshoro, 76080, Sindh, Pakistan

[b]Dr. M. A. Kazi Institute of Chemistry, University of Sindh, Jamshoro, 76080, Sindh, Pakistan. E-mail: zaffar.ibhupoto@usindh.edu.pk; aneelatahira80@gmail.com

[c]Mehran University of Engineering and Technology, 7680 Jamshoro, Sindh, Pakistan

[d]Université de Lorraine, CNRS, IJL, F-54000 Nancy, France

[e]Department of Metallurgy, NED University of Engineering and Technology, Karachi, Pakistan

[f]IMEM-CNR, Sede di Trento-FBK, Via alla Cascata 56/C, 38123 Trento, Italy

[g]Department of Chemistry, College of Science, King Saud University, Riyadh 11451, Saudi Arabia

[h]Institute of Physics University of Sindh, Jamshoro, 76080, Sindh, Pakistan

[i]Department of Pharmacognosy, College of Pharmacy, Arab Academy for Science, Technology and Maritime Transport, Alexandria 1029, Egypt

biosynthesis, the plants and extracts, animals, microorganisms, viruses, DNA, and proteins are widely used.[4–12] The superiority of biosynthesis to that of chemical and physical methods can be described in terms of green aspects with no toxicity to our environment, low cost in terms of use of pressure and energy during synthesis, and the nanostructured materials have excellent biocompatibility, stability, and homogeneity.[2,13–16] Therefore, the biomediated preparation of nanostructured materials is increasingly getting preference. Biosynthesis-based nanostructured materials have been studied for various energy conversion systems.[2,5,7]

Wastewater treatment is a very critical problem for a clean environment. Wastewater from different industries such as textiles, leather tanning, cosmetics, and food is associated with a wide range of synthetic dyes. These dyes are the main water pollution factors and a serious threat to the aquatic life and our environment.[17,18] Methylene blue is extensively used for dyeing fabrics, but it causes prolonged toxic effects on the human body. The most observed adverse effects of methylene blue on human health are allergies, mental disorders, dermatitis, cancer, and heart diseases.[19,20] Therefore, it is highly important

to develop low-cost, simple, and environment-friendly technologies that allow the efficient degradation of methylene blue.

Photocatalysis is considered to be a highly efficient technology for the degradation of dyes compared to other methodologies, including chemical, physical, and biological methods.[21–25] For this reason, photocatalysis is today defined as the most advanced technology for the degradation of water-soluble synthetic dyes.[23,26] The semiconducting material titanium dioxide (TiO_2) has been widely used as a promising photocatalyst,[27] and photocatalytic applications based on semiconducting materials have received significant attention ever since.[28–31] On the other hand, carbon materials such as carbon dots have proved to be excellent for photocatalytic applications due to their advantageous features such as unique internal and external sp^2 and sp^3 hybridized carbon orbitals.[32] Carbon dots exhibit numerous hydrophilic functionalities including hydroxyl, carboxyl, and epoxide. These properties of carbon dots enable them to be dispersed very well in polar solvents.[33] Furthermore, carbon dots exhibit attractive physical and chemical characteristics such as significant luminescence, chemical inertness, limited toxicity, outstanding conductivity, and water solubility.[34] Carbon dots are prepared using both top-down and bottom-up techniques, including carbonization or pyrolysis,[35,36] chemical oxidation,[37] arc discharge,[38] laser etching,[39] microwave,[40] and solvothermal/hydrothermal methods.[41,42] In recent times, the biosynthesis method is extensively used to produce nanosized carbon materials; for this purpose, various biomasses have been used to prepare carbon materials such as chest nuts,[43] coriander,[44] lemon peel,[45] cashew gum,[46] honey,[47] orange juice,[48] orange peels,[49] radish,[50] egg,[51] shrimp,[52] pitahaya,[53] milk,[54] apple juice,[55] stem of

banana plant,[56] pine apple peel,[57] citric acid,[58] corn and strawberry powder,[59] rosemary leaves,[60] and biomass (glucose, chitin, and chitosan).[61] These nanosized carbon materials have been utilized for biological, energy conversion, and environmental applications.[35] The biosynthesis method is simple, inexpensive, environment friendly, and highly desirable for the large-scale production of carbon-based materials. Currently, carbon dots are widely used for the degradation of synthetic dyes due to their intense light absorption, strong light trapping capacity, and minimal charge recombination rate of photogenerated electron–hole pairs.[62] An innovative, inexpensive, abundant, and environment friendly source of materials such as yogurt has not been reported so far in the existing scientific literature for the production of luminescent carbon materials.

In this study, we prepared an innovative green carbon material by carbonizing yogurt produced at a local dairy as an inexpensive, simple, and abundant source. The morphology, crystalline structure, and chemical and optical properties of the carbon material were investigated. The green and innovative carbon material was used to degrade methylene blue in an aqueous solution under the irradiation of ultraviolet light. Various degradation parameters were studied, such as the photocatalyst dose, initial dye concentration, and pH of the dye solution.

2. Experimental section

2.1. Synthesis of luminescent green and innovative carbon material

The yogurt was purchased in June from a local dairy shop located close to the University of Sindh Jamshoro, Sindh, Pakistan. In the
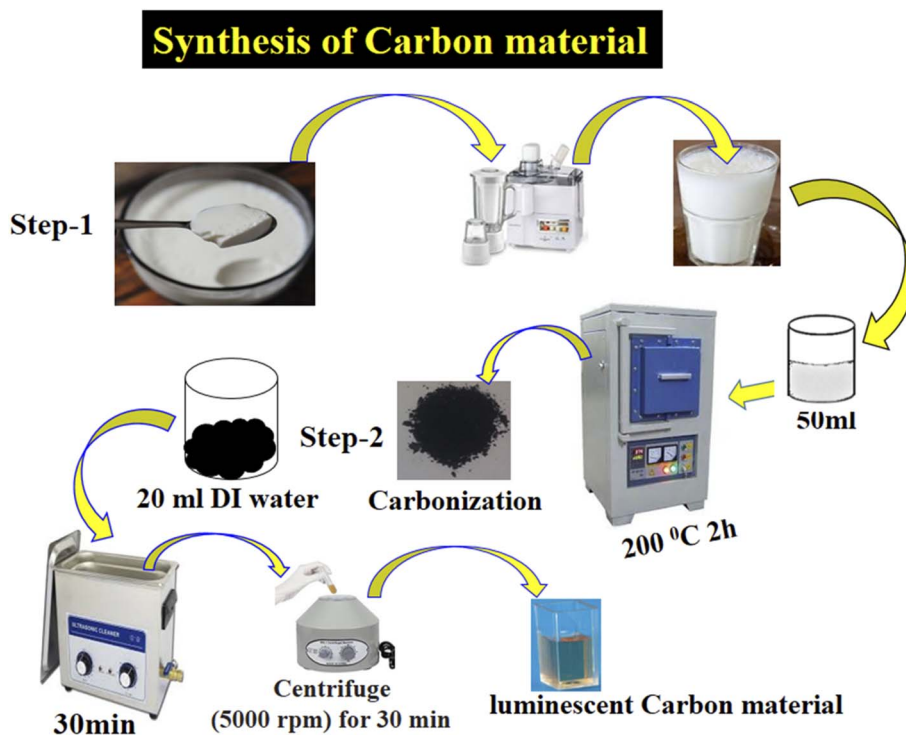
Scheme 1 Scheme of the green and innovative carbon material synthesis process.

typical synthesis of yogurt, the bacteria ferment the lactose sugar into lactic acid. Later, lactic acid makes the milk more acidic in nature, which helps the proteins to coagulate. Yogurt is rich with a variety of chemical compounds such as fat, protein, water, total solids, and ash. The pH of yogurt was about 4. The yogurt was more than 80% white, 1.5% greenish, and 8.86% yellowish and a very coagulated dense material. It was used in the carbonization process without any pretreatment. A typical preparation process of the luminescent carbon material from yogurt is described below and is shown in Scheme 1. The synthesis process consisted of two steps: (i) carbonization of yogurt and (ii) separation of the product by filtration. Initially, 40 mL yogurt was transferred to a 50 mL glass beaker, then carbonized at 200 °C for 2 h in a muffle furnace with a ramp rate of 15 °C min^{-1}. 3 g of the product obtained was dispersed in deionized water and sonicated for 40 min, and then filtered with a 0.2 μm filter membrane. The filtrate was then centrifuged at 5000 rpm for 30 min to remove the larger carbon particles. Finally, 0.5 g of a dark brown carbon material was successfully obtained. The morphology of the carbon material was studied by scanning electron microcopy (JSM-5910, JEOL) at a voltage of 20 kV. Fourier transform infrared spectroscopy was used to record different vibrational bands (Tensor 27, Bruker Optics FT-IR), and powder X-ray diffraction (Shimadzu-Model Kyoto, Japan) was used to investigate the crystalline structure of the carbon material with Cu/Kα radiation ($\lambda = 1.5406$ Å) at 45 kV and 45 mA.

2.2. Photocatalytic activity of the carbon material prepared from yogurt

The photocatalytic activity of the carbon material was evaluated for the degradation of the MB dye. Initially, different amounts of the catalyst (5, 10, and 15 mg) were added to 50 mL of the MB dye solution, and then stirred to form a homogeneous suspension. Each mixture was stirred in the dark for 30 min before establishing the adsorption–desorption equilibrium between the photocatalyst and the dye solution. Then, each dye solution with the photocatalyst was transferred to a homemade UV light box and irradiated with UV light to activate the catalyst. The homemade UV box consists of five light-emitting diodes (LEDs) with a wavelength of 365 nm and a power of 10 watts. During irradiation with UV light, 1 mL of each dye solution was taken at regular intervals and analyzed using a UV-vis spectrophotometer (Lambda 365, PerkinElmer). The UV-visible absorption spectra were recorded from 200 to 800 nm at different time intervals. The optimal wavelength of 664 nm is related to the intrinsic absorbance wavelength of the MB dye.

The photocatalytic degradation efficiency (% C_{deg}) of the carbon material was calculated using the following equation.

$$\% \ C_{deg} = \frac{C_0 - C_t}{C_0} \times 100\%, \ \ 0 \le t \le 6 \tag{1}$$

where C_o and C_t are the MB concentration at the beginning and after reaching the adsorption–desorption equilibrium, respectively. The photodegradation kinetics of the MB dye by means of the carbon material was evaluated through the Langmuir–Hinshelwood equation[63] as follows.

$$-\ln\left(\frac{C_0}{C_t}\right) = Kt, \ \ 0 \le t \le 60 \tag{2}$$

where K_t denotes the rate constant for the pseudo-first order model.

To understand the effect of pH on the degradation process, we adjusted the pH of various MB solutions to 5, 7, 9, and 11. The pH adjustment of the dye solutions was performed with 0.2 M NaOH and 0.2 M HCl solutions.

2.3. Radical scavenger experiment

Scavenging experiments were carried out to detect the main reactive species during the photocatalytic decomposition of MB. For this purpose, ascorbic acid ($C_6H_8O_6$), ethylenediamine tetracetate acid disodium (EDTA-Na$_2$), and sodium monohydrate (NaBH$_4$) scavengers were added to the MB solution, and the corresponding absorbance spectra were collected. 60 μL of each scavenger at a concentration of 10 mM was added to the MB solution together with 15 mg of the photocatalyst. The experiment was conducted for 210 min under illumination with UV light.

The electrochemical active surface area (ECSA) experiment of the as-prepared carbon material was performed with cyclic voltammetry at different scan rates. For the electrochemical experiments, we built a three-electrode cell of silver–silver chloride (Ag/AgCl) filled with 3 M KCl electrolytic solution as the reference electrode, platinum wire as the counter electrode, and modified glassy carbon electrode as the working electrode. The cleaning of the glassy carbon electrode was done with 3 μm alumina paste solution and silicon paper, followed by washing with deionized water. The glassy carbon electrode was modified with the 5 mg dispersed carbon material ink in the mixture of deionized water and 50 μL of 5% Nafion solution. Then, 10 μL (0.2 mg) of carbon ink was drop casted on the (0.03 cm^2) surface area of glassy carbon electrode and dried with a blow of air at room temperature. Electrochemical impedance spectroscopy (EIS) was carried out with measurement conditions of 50 kHz to 0.1 Hz frequency, amplitude of 5 mV, and zero biasing potential. All the electrochemical measurements were done in 2.3 × 10^{-5} M solution of MB on a Versa potentiostat. The current density was calculated by dividing the measured current with the surface area of the glassy carbon electrode. The obtained EIS spectrum was simulated with Z-view software for the fitted equivalent circuit and estimated the charge transfer resistance. The particle size distribution was calculated by dispersing 2 mg of the carbon material in 20 mL of deionized water using a Malvern Zetasizer Nano (zs).

3. Results and discussion

3.1. Structural characterization of the carbon material prepared from yogurt

The morphology of the carbon material was investigated by scanning electron microscopy (SEM), and the SEM images at different magnifications are shown in Fig. 1a and b. The SEM images describe a structure consisting of large sheets (Fig. 1a) composed of small particles, whereas those in Fig. 1b suggest
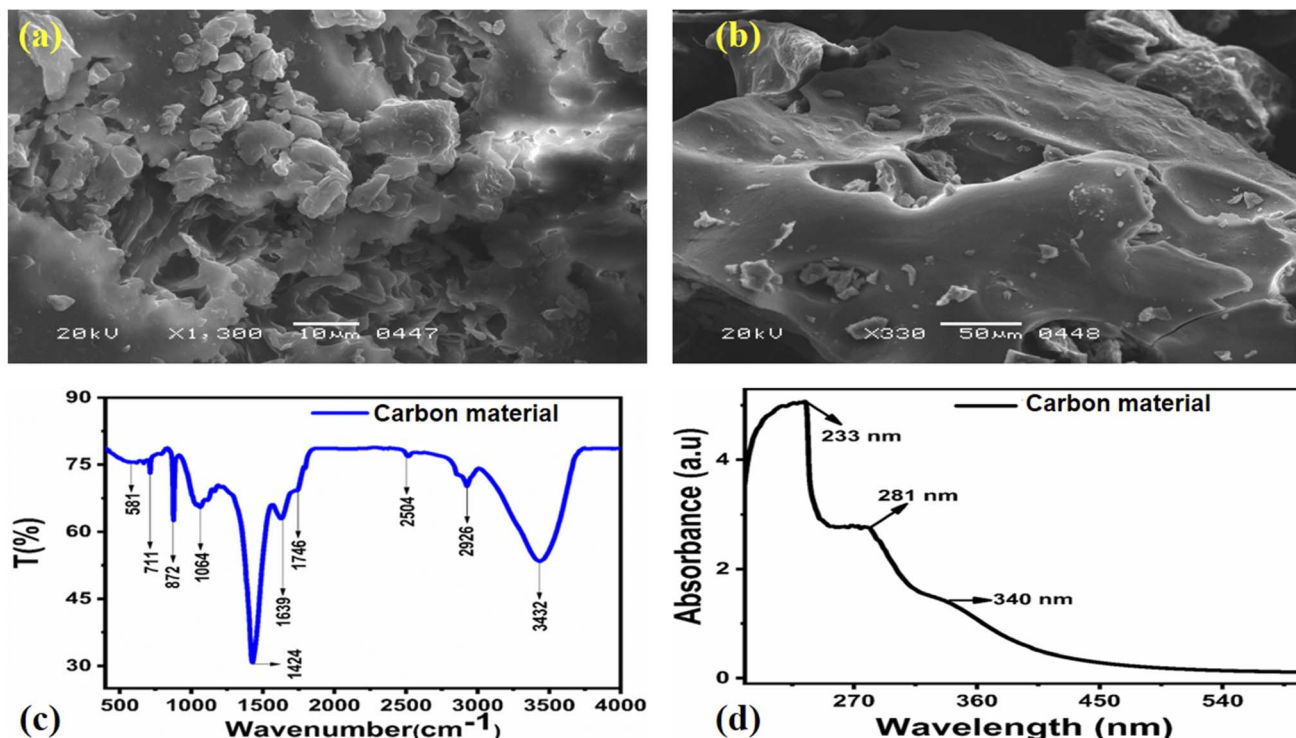
Fig. 1 (a, b) SEM images of the green and innovative carbon material at different magnifications, (c) FTIR spectrum of the carbon material, (d) UV-visible absorbance spectrum of the carbon material.

that the material prepared from natural yogurt has graphitic aspects typical of carbon dots. Furthermore, the SEM analysis revealed a uniform size distribution of the carbon material. FTIR analysis was performed to identify the presence of functional groups on the surface of the carbon dots, as shown in Fig. 1c. The presence of a large band at 3432 cm^{-1} was assigned to hydroxyl groups (O–H) adsorbed on the surface, while the low peak at 2926 cm^{-1} was attributed to the stretching vibration of the C–H chemical bond. A very weak peak at 2504 cm^{-1} is related to the stretching vibrational frequency of SH, while the weak peak at 1746 cm^{-1} is attributed to the stretching vibrational frequency of the C=O bond. The peak at 1639 cm^{-1} corresponds to the stretching vibration of C–O and the bending mode of N–H,[64] while the one at 1424 cm^{-1} is related to the stretching frequency of the C–N, N–H, and –COO chemical

bonds. These observations confirm that reducing groups including –OH, –NH$_2$, and –COO are localized on the surface of the carbon dots, in full agreement with various works reported for fluorescent carbon dots.[65–68]

The UV-visible spectrum of the aqueous solution of carbon material is shown in Fig. 1d, where a slight shoulder at 340 nm (3.6 eV) related to the n–π* transition of C=O is visible.[69] Three characteristic peaks in the 200–400 nm range are visible, at 233 nm, 281 nm, and 340 nm. The absorption bands at 233 and 281 nm come from the sp^2 hybrid orbitals of aromatic carbon, belonging to its π–π* transition.[70] A broad absorption shoulder at 340 nm is related to the C=O bond, revealing the n-π* transition, in good agreement with the reported work.[71,72] The UV-visible spectroscopic analysis revealed that the prepared material has characteristics similar to those of carbon dots reported in previous works.[71,72] The crystalline structure of the material was also studied through the powder XRD technique, and the obtained pattern is shown in Fig. 2, in which the XRD diffraction peaks at 19.63°, 28.25°, 44.56°, 65.05°, and 70.06° are visible. The peak at 19.63°, relative to the (001) planes is hardly visible, while the one at 28.25°, relative to the (002) planes, is sharper. Finally, the one at 44.56°, relative to the planes (101), is clear and intense. The presence of these peaks confirms that the material has crystalline characteristics corresponding to graphite, which is entirely in agreement with the work reported on carbon dots.[73] The inset in Fig. 2 shows the camera image of the luminescent carbon material obtained from yogurt. The carbon material was poured into the quartz glass cuvette, then
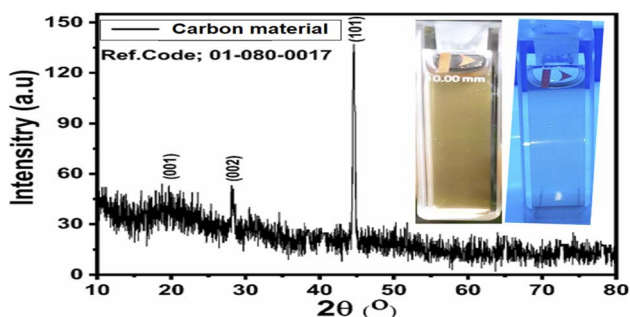

Fig. 2 XRD diffraction patterns of the carbon material obtained from yogurt; the inset shows the luminescent aspects of the carbon material.

the UV light was irradiated for 5 min, and a camera was used to take the picture.

3.2. Photodegradation of methylene blue in an aqueous solution under illumination with UV light using the carbon-based material

The photocatalytic activity of the carbon-based material was tested for the photodegradation of methylene blue in an aqueous solution under illumination with UV light. Various parameters were studied to evaluate the photocatalytic performance of the prepared carbon-based material, such as the initial dye concentration, photocatalyst amount, and pH of the MB aqueous solution.

3.2.1. Effect of initial MB dye concentration and different doses of the photocatalyst.
To verify the performance of the photocatalyst obtained from yogurt as a function of the dye concentration, we tested it at two different MB dye concentrations, namely 2.3×10^{-5} M and 0.7×10^{-5} M. Solutions with different amounts of the carbon photocatalyst (5, 10, and 15 mg) were irradiated with UV light over time, and the absorption spectra of the dye were compared with those before the photocatalysis process.

First, we studied the effect of different amounts of the photocatalyst (5, 10, and 15 mg) at a low concentration of MB (0.7×10^{-5} M) under UV light illumination for 140 min, collecting an absorption spectrum every 20 min, as shown in Fig. 3. The absorbance spectra of all the three solutions showed a decrease in the MB peak over time and showed almost complete degradation within 140 min. These results show that for a low concentration of MB, $i.e.$, 0.7×10^{-5} M, the carbon material prepared from yogurt is exceptionally effective in degrading MB in the aqueous solution. We then investigated the performance

of various photocatalyst amounts (5, 10, and 15 mg) on a higher concentration of MB dye (2.3×10^{-5} M), as shown in Fig. 4. In this case, the peak decreases much more slowly. Furthermore, the solution with 15 mg catalyst shows the highest degradation efficiency with a value of 94.8%. This demonstrates that increasing the amount of the catalyst significantly affects the photodegradation kinetics. However, the performance of 15 mg carbon material has a slightly lower degradation efficiency than it does on the lower concentration of MB. This could be attributed to the fact that 2.3×10^{-5} M concentration could shield the UV light during the process, limiting the number of photons that reach the surface of the carbon material. This would lead to a lower production of electron–hole pairs, low amount of oxidizing radicals, and therefore, to a lower degradation efficiency.

3.2.2. Effect of pH of the MB dye solution.
The pH of the dye solution is one of the critical factors in the degradation efficiency.[74] Using the MB solution at 2.3×10^{-5} M concentration, a more convincing test was considered, 15 mg photocatalyst were tested at different pH values (5, 7, 9 and 11) under UV light for 160 min. We prepared 100 mL MB solution at a concentration of 2.3×10^{-5} M, and then four solutions with different pH values were obtained by adding an appropriate amount of 0.2 M NaOH or HCl solution. The pH of the dye solution increased to 6.5, 8.8, 10.9, and 12.4 after degradation for the initial pH values of 5, 7, 9, and 11, respectively, indicating the enhancing effect of the photocatalytic reaction at different pH values. 15 mg carbon material was added to each solution at different pH values, and the solutions were stirred for 160 min at room temperature, as shown in Fig. 5. The highest percentage of dye removal was 98.4% for the dye solution with a pH of 11. This can be attributed to the high density
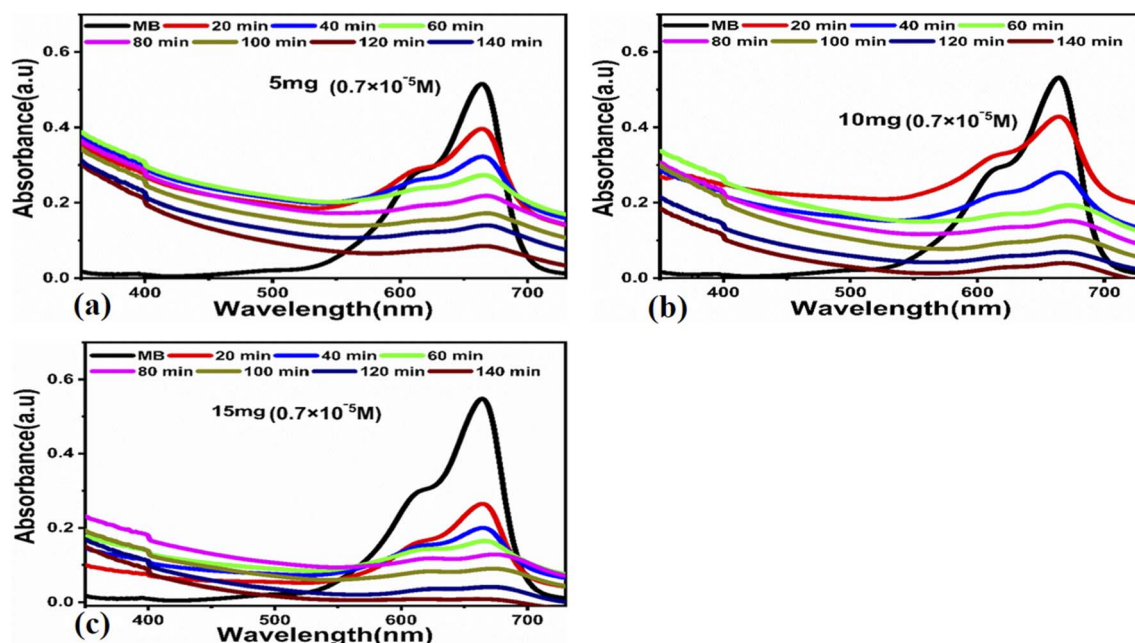

Fig. 3 UV-visible absorbance spectra at an MB concentration of 0.7×10^{-5} M for the time interval of 140 min under the irradiation of UV light (a) a catalyst dose of 5 mg, (b) a catalyst dose of 5 mg, (c) a catalyst dose of 5 mg.

Fig. 4 UV-visible absorbance spectra at an MB concentration of 2.3×10^{-5} M for the time interval of 210 min under the irradiation of UV light (a) a catalyst dose of 5 mg, (b) a catalyst dose of 10 mg, (c) a catalyst dose of 15 mg.
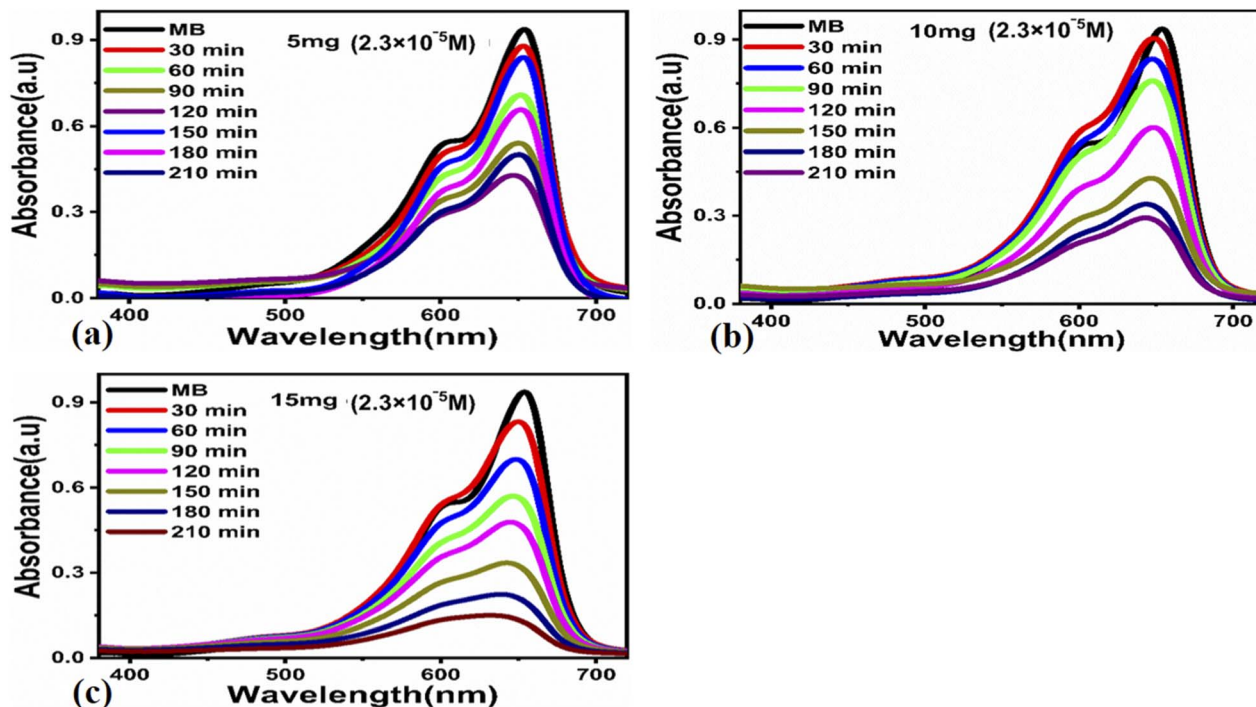
of hydroxyl ions under higher alkaline conditions, which could act as oxidizing radicals actively involved in the degradation process. Moreover, a possible reason for the higher degradation rate of MB under alkaline conditions is associated with the enhanced dissolving capability of unprotonated MB solution.[75] Hydroxyl radicals are produced during photocatalysis *via* the reaction of hydroxide ions with positively charged holes under alkaline pH conditions.[75] Hydroxyl radicals strongly support the
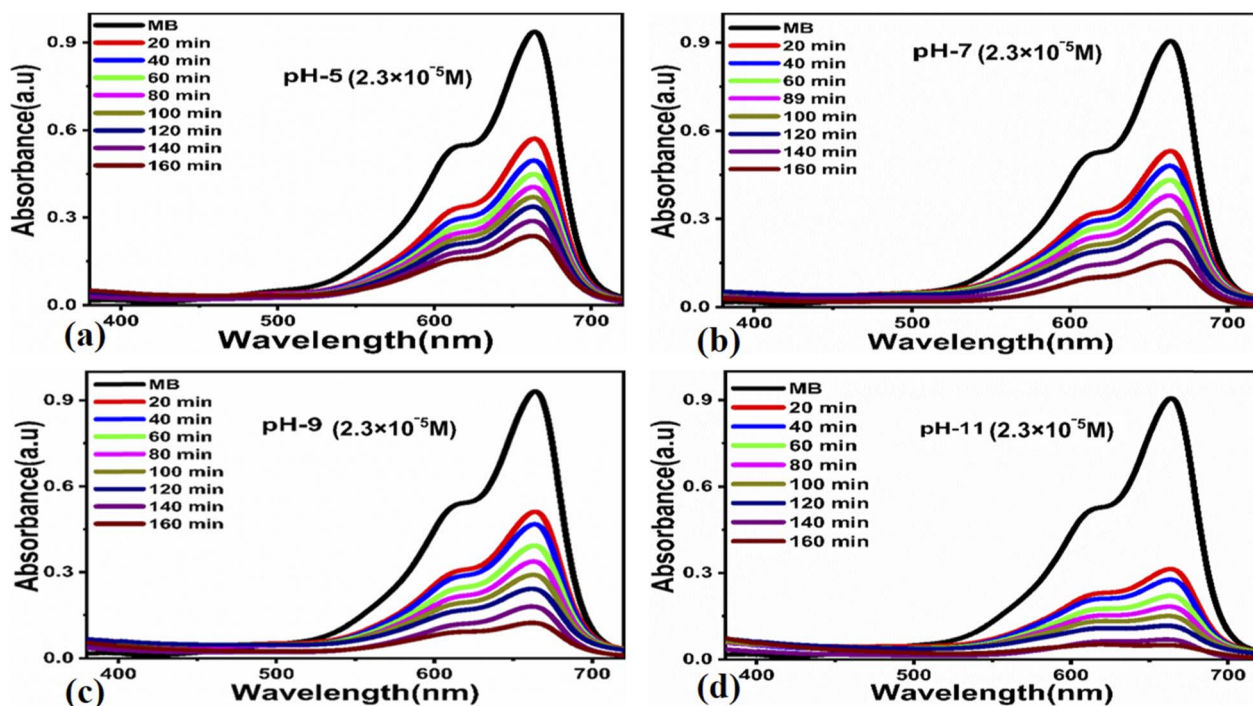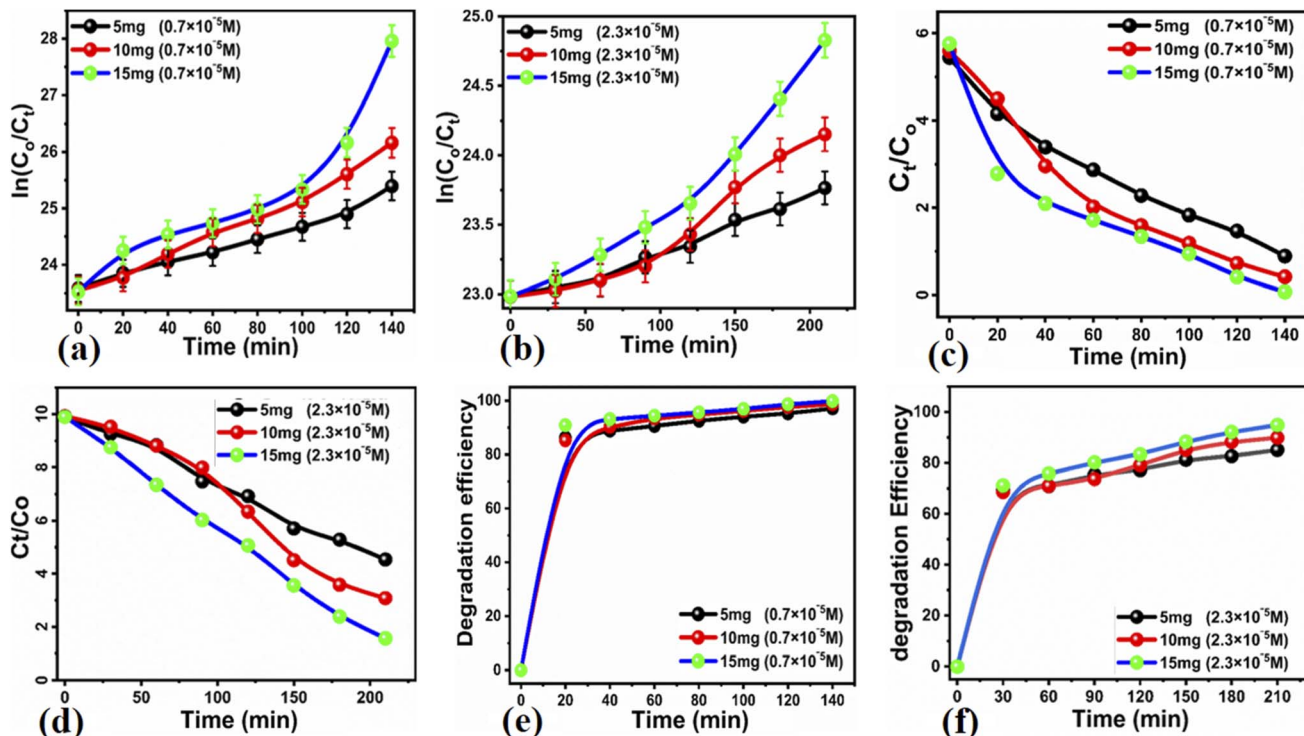

Fig. 5 UV-visible absorbance spectra at an MB concentration of 2.3×10^{-5} M at different pH values of the dye solution for the time interval of 160 min under the irradiation of UV light using a catalyst dose of 15 mg (a) pH 5, (b) pH 7, (c) pH 9, (d) pH 11.

Fig. 6 Evaluation of degradation kinetics (a) linear plot of the natural logarithm of concentrations such as C_0 initial and C_t after certain intervals of time at an MB concentration of 0.7×10^{-5} M with various catalyst doses of 5, 10, and 15 mg for the time interval of 140 min, (b) linear plot of natural logarithm of concentrations such as C_0 initial and C_t after certain intervals of time at an MB concentration of 2.3×10^{-5} M with various catalyst doses of 5, 10, and 15 mg for the time interval of 210 min, (c) linear plot of concentrations such as C_0 initial and C_t after certain intervals of time at an MB concentration of 0.7×10^{-5} M with various catalyst doses of 5, 10, and 15 mg for the time interval of 140 min, (d) linear plot of concentrations such as C_0 initial and C_t after certain intervals of time at an MB concentration of 2.3×10^{-5} M with various catalyst doses of 5, 10, and 15 mg for the time interval of 140 min, (e) degradation efficiency of the MB concentration 0.7×10^{-5} M with various catalyst doses of 5, 10, and 15 mg for the time interval of 140 min, (f) degradation efficiency of the MB concentration 2.3×10^{-5} M with various catalyst doses of 5, 10, and 15 mg for the time interval of 210 min.

degradation of MB through the oxidation of hydroxide ions on the surface of the carbon-based material.[76] Furthermore, it has been found that the effectiveness of photocatalysis at different pH values is strongly dependent on the nature of the photocatalytic material.[77] However, at low pH, the relative concentration of hydroxyl ions is lower; therefore, a lower degradation rate is observed.

3.2.3. Kinetics study of methylene blue degradation. The degradation kinetics of low and high concentration methylene blue were studied with different amounts of the catalyst, as reported in Fig. 6. From the first order reaction kinetics, the

value of the rate constant (K) can be estimated through the equation $\ln(C_t/C_0) = kt$. Here, C_t and C_0 are the dye concentration at a certain time "t" and at the beginning of the reaction (initial concentration), respectively. The rate constant values, reported in Table 1, show that the photodegradation rate is faster at a low concentration of MB than at higher concentrations. The MB degradation rate using the carbon material obtained from yogurt is comparable or higher than that of many nanostructured materials reported in recent works.[78] The degradation efficiency using 15 mg of the carbon material is higher (99.7%) at low MB concentrations, as shown in Fig. 5e,

Table 1 Summary of the obtained results with the carbon material obtained from yogurt

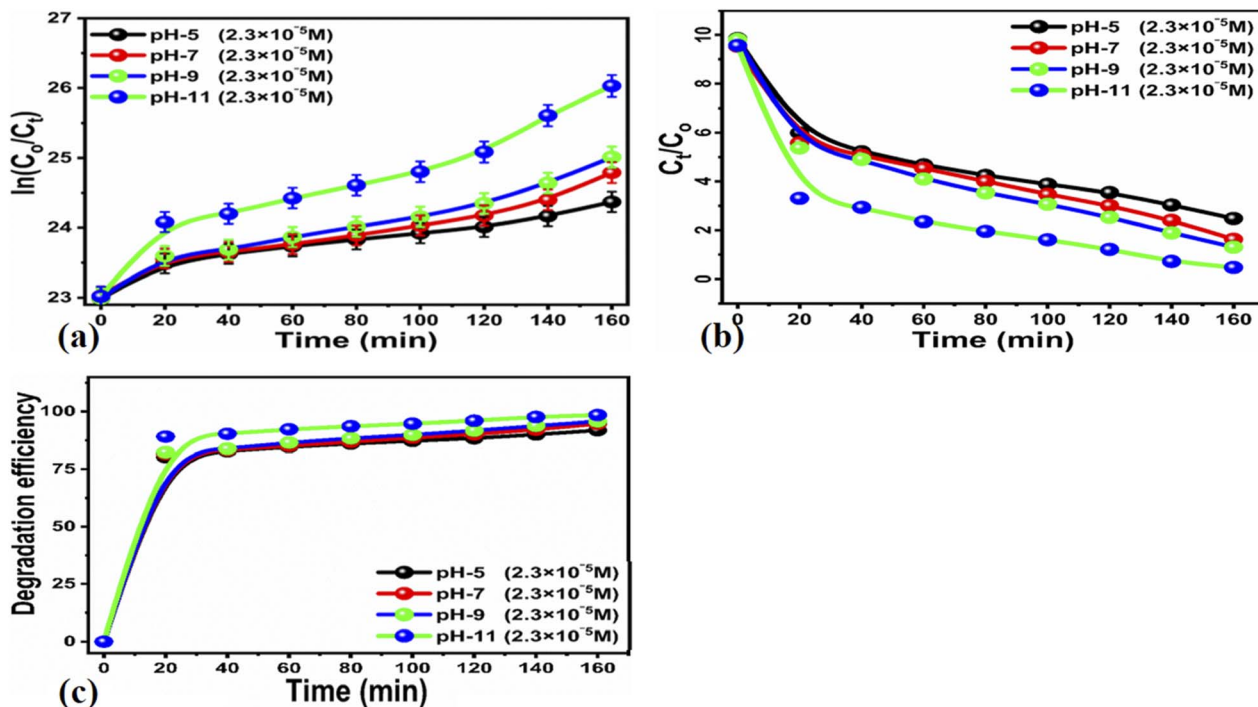| Sample dose (mg)	Dye conc	Constant (K)	Dye conc	Constant (K)	Scavengers	Constant (K)
5	2.3×10^{-5} M	3.83×10^{-3} min^{-1}	0.7×10^{-5} M	1.19×10^{-2} min^{-1}	EDTA	2.80644×10^{-4}
10		6.08×10^{-3} min^{-1}		1.80×10^{-2} min^{-1}	$C_6H_8O_6$	3.93772×10^{-4}
15		6.63×10^{-3} min^{-1}		2.57×10^{-2} min^{-1}	NaBH$_4$	3.45494×10^{-4}
pH study						
pH 11	2.3×10^{-5} M	7.10×10^{-3} min^{-1}				
pH 9		9.10×10^{-3} min^{-1}				
pH 7		1.06×10^{-2} min^{-1}				
pH 5		1.56×10^{-2} min^{-1}				

Fig. 7 The evaluation of degradation kinetics (a) linear plot of the natural logarithm of concentrations such as C_0 initial and C_t after certain intervals of time at an MB concentration of 2.3×10^{-5} M with 15 mg for the time interval of 150 min for pH values 5, 7, 9, and 11, (b) linear plot of concentrations such as C_0 initial and C_t after certain intervals of time at an MB concentration of 2.3×10^{-5} M with catalyst dose of 15 mg for the time interval of 150 min for pH values 5, 7, 9, and 11, (c) degradation efficiency of the MB concentration of 2.3×10^{-5} M with a catalyst dose of 15 mg for the time interval of 150 min for pH values 5, 7, 9, and 11.

while it is lower but still good (94.8%) at higher concentrations, as shown in Fig. 5f. These values indicate significantly enhanced photocatalytic properties of the carbon material compared to previous works.[79–81] Similarly, the study of MB degradation kinetics was also carried out at various pH values of the dye solution (at a concentration of 2.3×10^{-5} M). The degradation kinetics at various pH values are shown in Table 1. In an acidic environment, there is a larger amount of holes that consequently accelerates the degradation kinetics. However, the

degradation is relatively slow at low pH due to the possible agglomeration of the carbon material (and therefore, the decrease of the catalyst surface), which leads to the poor absorption of UV photons. In addition, the high density of cationic protons under acidic conditions creates a strong repulsion between the molecules of MB itself, which can reduce the interaction of MB with the catalyst surface, and therefore, also the degradation of the dye. In an alkaline environment, there is a high probability of generation of hydroxyl radicals
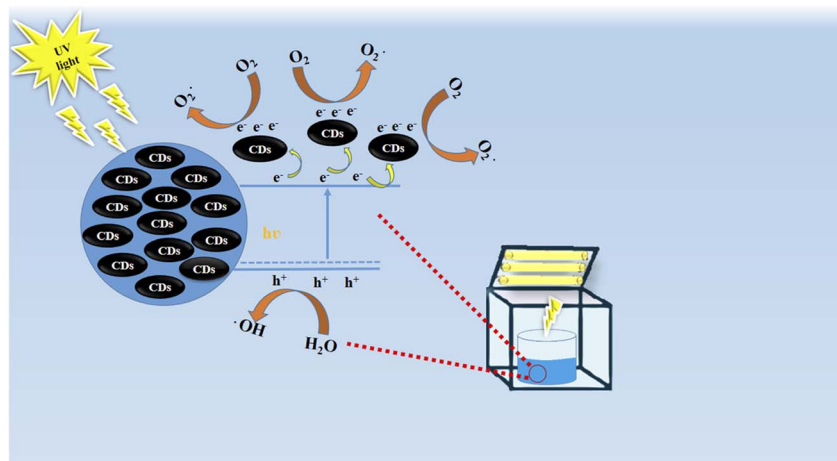
Scheme 2 The proposed reaction mechanism of MB adsorption onto luminescent carbon material prepared from yogurt.

Table 2 Comparative analysis of the proposed study with the published results on the degradation of MB

Catalyst	Dye	% Removal	Time (min)	Light source	Ref.
Bio-CDs	Methylene blue	94.2%	45	Visible light	88
N-CQDs	Methylene blue	97%	260	UV light	89
TiO_2-CQDs	Rhodamine-B	77%	150	Visible light	90
NCQDs	Methylene blue	77%	90	Sun light	91
NCQDs/TiO_2	Methylene blue	86.9%	420	Visible light	92
S,N-CQDs/TiO_2	Acid red 88	77.2	180	Visible light	93
CDs/TiO_2	Methylene blue	90%	120	Visible light	94
CQDs/Bi_2MoO_6	Rhodamine-B	97.1%	50	Solar light	95
Cl-CQDs	Methylene blue	56%	240	Solar light	96
CQDs	2-Nitrophenol (2-NP)	80.79%	120	Sun light	97
CQDs	Methyl orange	68.9%	120	Visible light	98
TiO_2-MCDs	Methylene blue	83%	120	Visible light	99
G-CDs	Methyl violet	63.6%	90	Visible light	100
Luminescent carbon material	Methylene blue	99.7%	140	UV light	Present work

(HO•HO•), which greatly help to degrade the dye. Under highly alkaline conditions, the surface of the carbon material can be negatively charged and promote the adsorption of MB, leading to more efficient photodegradation (Fig. 7).

3.2.4. Degradation mechanism of MB on the carbon material. The degradation mechanism of MB on the carbon material obtained from yogurt under UV light irradiation is shown in Scheme 2. The irradiation with UV light can produce radicals such as •OH and $O_2^{•-}$, which would be actively involved in the degradation of MB, resulting in numerous intermediates that eventually decompose into several nontoxic compounds including SO_3, NO_2, NH_2, CH_4, H_2O, and CO_2. Existing literature shows that the degradation of MB is accompanied by the dissociation of the chromophoric structure and the decomposition of homo- and heterolytic aromatic cycles of MB.[82] The carbon material is excited during UV light irradiation and as a result, radicals might be produced, which contribute to the degradation of the MB. This is possible due to the availability of numerous electron–hole pairs with adequate energy of the conduction or valence bands; consequently, a high flow of
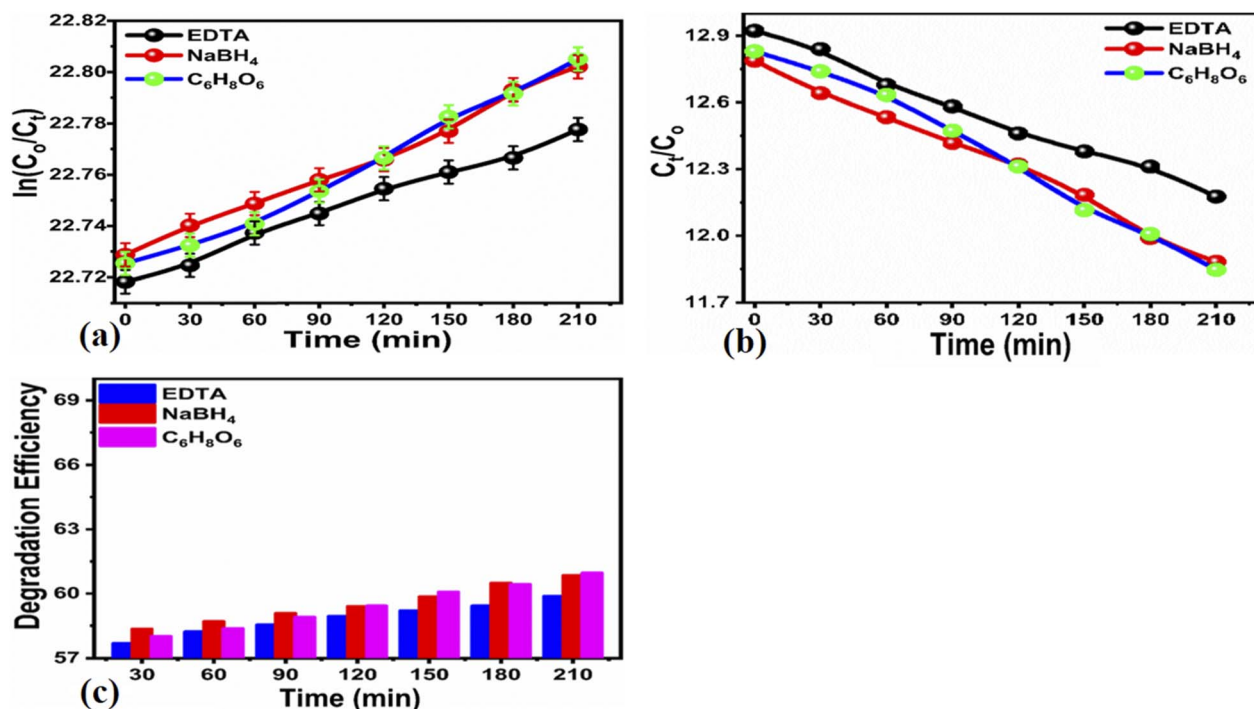

Fig. 8 Evaluation of the degradation kinetics (a) linear plot of the natural logarithm of concentrations such as C_0 initial and C_t after certain intervals of time at an MB concentration of 2.3×10^{-5} M with 15 mg for the time interval of 210 min in the presence of different scavengers, (b) linear plot of concentrations such as C_0 initial and C_t after certain intervals of time at an MB concentration of 2.3×10^{-5} M with a catalyst dose of 15 mg for the time interval of 210 min in the presence of different scavengers, (c) degradation efficiency of MB under the environment of different scavengers at an MB concentration of 2.3×10^{-5} M using a catalyst dose of 15 mg under the irradiation of UV light.

electrons and holes is possible due to their separation at the time of MB degradation under UV light irradiation. Unfortunately, when we tested the photocatalyst under natural sunlight, we found that the degradation performance of MB is limited compared to that achieved under UV light (Table 2).

3.2.5.   Scavenger study. The kinetics of MB degradation was also evaluated in the presence of various scavengers and the reaction kinetics followed the pseudo-first order mechanism, as shown in Fig. 8a and b. The scavenger agents tested were ascorbic acid, sodium borohydride, and ethylenediamine tetraacetate (EDTA). Active radicals such as superoxide radical ions ($^{\bullet}O^{2-}$), hydroxyl radicals ($^{\bullet}OH$), and photogenerated holes (h^{+}) have been found to be involved in the degradation process. These selected scavengers are mainly linked to ($^{\bullet}O^{2-}$) and hydroxyl radicals ($^{\bullet}OH$),[83] and the degradation of MB mainly depends on the amount of these oxidizing species, as previously reported in several studies.[84,85] The degradation rate of MB was greatly reduced using EDTA as a scavenger, revealing that hydroxyl radicals play an important role in the degradation of MB under alkaline conditions, as shown in Fig. 8c. For understanding the role as a carbon material toward the degradation of MB, we have also studied the degradation of 2.3×10^{-5} M MB solution under the illumination of UV light without the use of a photocatalyst, as shown in Fig. 9. The UV-visible absorption spectra suggest a negligible effect on the dye degradation, as confirmed from the low absorbance value, as shown in Fig. 9a. The reaction kinetics was further studied, as shown in Fig. 9b

and c, indicating that the UV light has limited effect on the reaction rate. The degradation efficiency of MB was observed to be about 6 to 7%, confirming that UV light itself has a negligible effect on the dye degradation efficiency, as shown in Fig. 9d. Therefore, the synthesis of potential photocatalysts is an immediate need for the efficient wastewater treatment process prior to the release of wastewater into the environment from various industrial sectors. The stability of the as-prepared carbon material was also evaluated after three cycles, as shown in Fig. 10. The initial dye degradation cycle is enclosed in Fig. 10a. Fig. 10b and c are two reusability cycles for the photodegradation of MB under the illumination of UV light, and it can be seen that the prepared carbon material has significant effectiveness even after three cycles, confirming the good stability of the material. The relative degradation efficiencies of three cycles are shown in Fig. 10d. The degradation efficiency of cycle-1, cycle-2, and cycle-3 is 93.3%, 90.2%, and 88.3%, respectively, which is acceptable for a low cost, earth abundant, innovative, and green approach. Further, to strengthen the performance of the as-prepared carbon material, we have analyzed the carbon sample by electrochemical active surface area studies and impedance spectroscopy, as shown in Fig. 11. Both the electrochemical measurements were done according to our previous work.[86] The electrochemical active surface area was calculated by cyclic voltammetry at various scan rates, as shown in Fig. 11a. The linear fitting of the current density of the anode and cathode sides of the CV curves was carried out, and
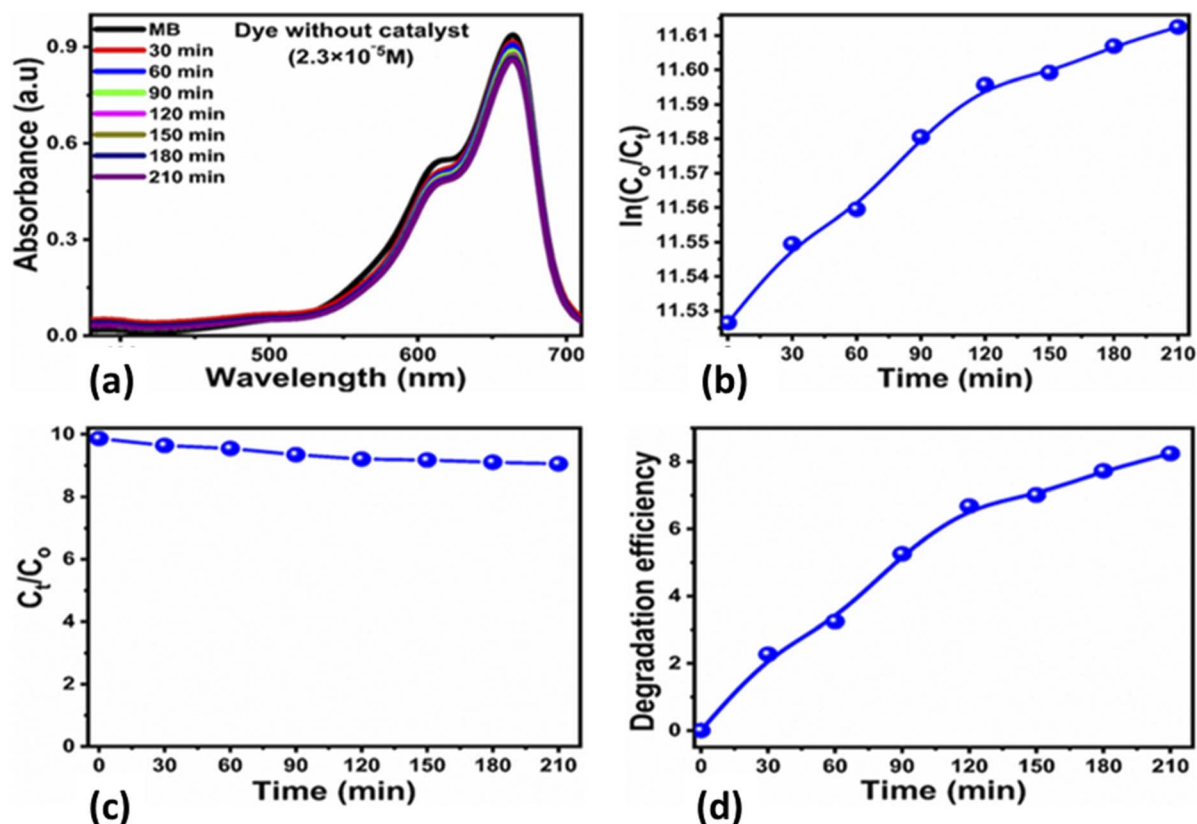

Fig. 9   (a) UV-visible absorbance spectra of the MB concentration of 2.3×10^{-5} M without the use of the photocatalyst for the time interval of 210 min under the irradiation of UV light, (b, c) reaction kinetics with the photocatalyst, (d) degradation efficiency without the photocatalyst.
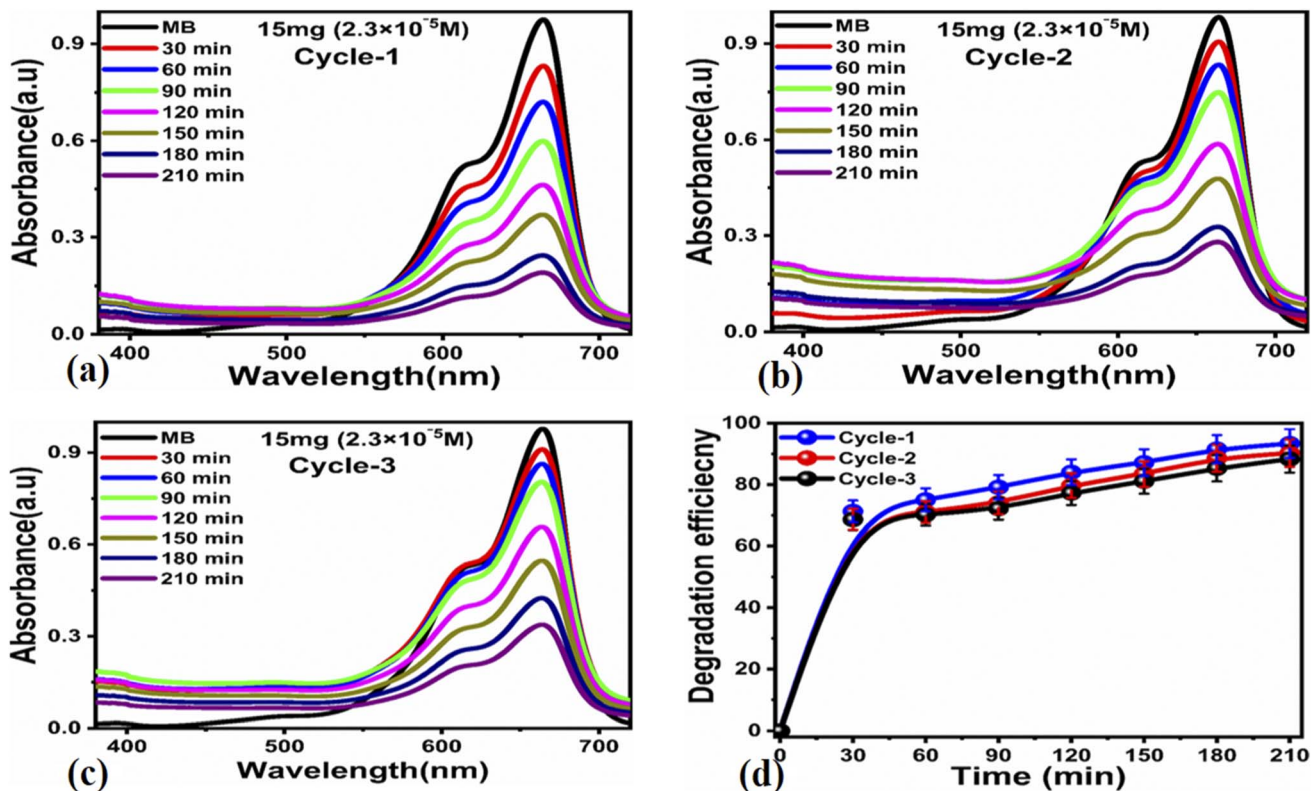
Paper

RSC Advances

Fig. 10 UV-visible absorbance spectra at an MB concentration of 2.3×10^{-5} M for understanding the reusability of the carbon material for a time interval of 160 min under the irradiation of UV light using a catalyst dose of 15 mg (a) cycle-1, (b) cycle-2, (c) cycle-3, (d) % photodegradation efficiency.

the obtained slope value from the fitting data was described as the suggested value of the electrochemical active surface area (ECSA), as shown in Fig. 11b. The obtained result of slope = 0.01 μ cm^{-2} confirms that the active surface area of the carbon material is significant and evidently supported the efficient

degradation performance of the carbon material toward the MB degradation process. The EIS was also employed to determine the charge transfer of the material, which could support the performance of the as-prepared carbon material, as shown in Fig. 11c. The EIS data was simulated and the equivalent circuit

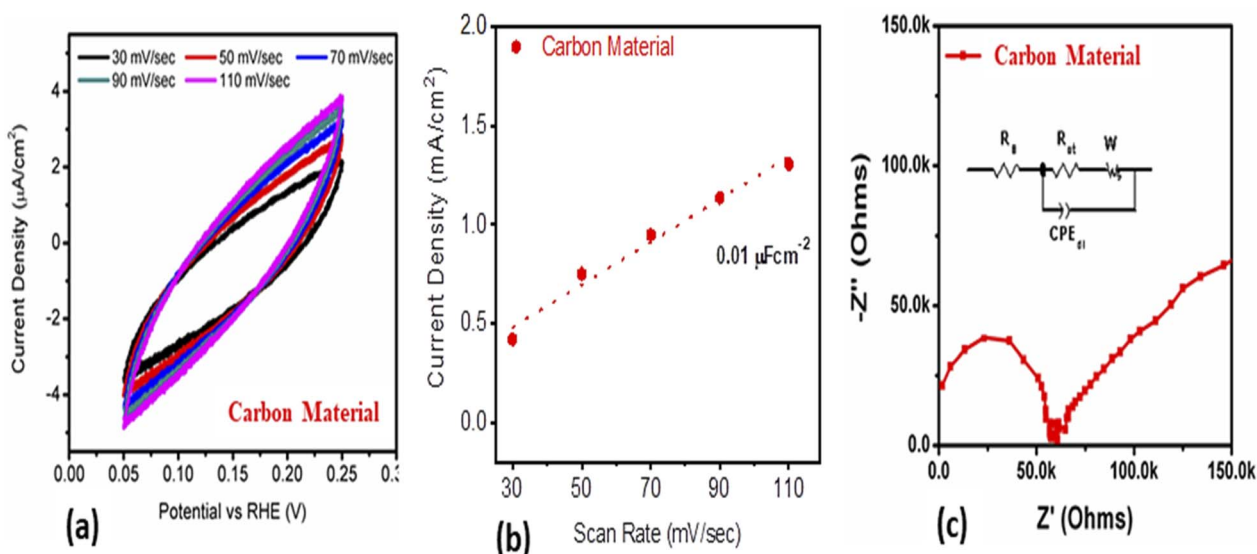**Fig. 11** (a) Cyclic voltammetry curves at various scan rates in 2.3×10^{-5} M solution of MB, (b) linear fitting of the current density at various scan rates, (c) EIS spectrum of the as-prepared carbon material in 2.3×10^{-5} M solution of MB.
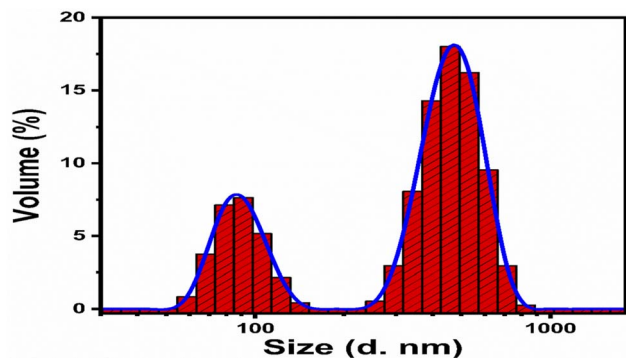
Fig. 12 Particle size distribution of the as-prepared carbon material from yogurt using a nanosizer.

with well-defined circuit elements is shown in the inset of Fig. 11c. The circuit elements such as solution resistance, carbon material film resistance, constant phase elements, and the Warburg constants were determined. The estimated value of charge transfer resistance of the carbon material was 50.115 K ohms from the simulation, which is close to the value of the reported photocatalyst.[87] In addition, the semicircle arc of the Nyquist plot is another evidence to estimate the material charge transfer resistance value. The EIS study has verified that the as-prepared carbon material from yogurt exhibits excellent avenues of charge transfer during the reaction, which could foster the reaction kinetics of MB degradation. Moreover, the particle size distribution of the as-prepared carbon material was also measured, as shown in Fig. 12. The particle size distribution was experimentally obtained using a Zetasizer Nano (ZS), and the average particle size was found to be 355 nm. However, the relative concentration of small size particles was low compared to the large particles in the sample. The particle size distribution suggests that the prepared carbon material exhibits a nanosize; therefore, it is shown in the literature that the material having nanosize has more surface area and, consequently, enhanced photocatalytic activity.

4. Conclusion

In this study, we synthesized a luminescent carbon material from yogurt through a green and innovative method of direct combustion in a muffle furnace. The SEM images and XRD patterns showed that the carbon material has similar morphology and structure to those of carbon dots. The UV-visible spectra confirmed that the carbon material exhibits luminescent characteristics. The carbon material was found to be highly active in the degradation of methylene blue under UV light irradiation. Various aspects of the photocatalyst were studied such as the catalyst dose, initial dye concentration, and pH of the dye solution. Furthermore, under alkaline conditions, MB was degraded even more efficiently. The scavenger studies confirmed that the hydroxyl radicals are the potential species for the efficient degradation of MB using the carbon material prepared from yogurt. The reusability and particle size distribution were also investigated. The production of luminescent

carbon materials from innovative green natural resources such as yogurt can be of great use for various photocatalytic applications.

Conflicts of interest

Authors declare no conflict of interest in this research work.

Acknowledgements

References

1 A. Rana, K. Yadav and S. Jagadevan, A comprehensive review on green synthesis of nature-inspired metal nanoparticles: mechanism, application and toxicity, *J. Clean. Prod.*, 2020, **272**, 122880.

2 S. Kaviya, Synthesis, self-assembly, sensing methods and mechanism of bio-source facilitated nanomaterials: a review with future outlook, *Nano-Struct. Nano-Objects*, 2020, **23**, 00498.

3 M. Nasrollahzadeh, M. Sajjadi, S. Iravani and R. S. Varma, Green-synthesized nanocatalysts and nanomaterials for water treatment: current challenges and future perspectives, *J. Hazard. Mater.*, 2021, **401**, 123401.

4 K. Dhanaraj and G. Suresh, Conversion of waste sea shell (Anadara granosa) into valuable nanohydroxyapatite (nHAp) for biomedical applications, *Vacuum*, 2018, **152**, 222–230.

5 W. C. Records, Y. Yoon, J. F. Ohmura, N. Chanut and A. M. Belcher, Virus-templated Pt–Ni(OH)$_2$ nanonetworks for enhanced electrocatalytic reduction of water, *Nano Energy*, 2019, **58**, 167–174.

6 H. Chandra, P. Kumari, E. Bontempi and S. Yadav, Medicinal plants: treasure trove for green synthesis of metallic nanoparticles and their biomedical applications, *Biocatal. Agric. Biotechnol.*, 2020, **24**, 101518.

7 G. Dong, H. Wang, Z. Yan, J. Zhang, X. Ji, M. Lin, R. A. Dahlgren, X. Shang, M. Zhang and Z. Chen, Cadmium sulfide nanoparticles-assisted intimate coupling of microbial and photoelectrochemical processes: mechanisms and environmental applications, *Sci. Total Environ.*, 2020, **740**, 140080.

8 K. Zhang, X. Wang, C. Long, J. Xu, Z. Jiang, B. Feng, P. Zhang, J. Fei and T. Qing, DNA/RNA chimera-templated copper nanoclusters for label-free detection of reverse transcription-associated ribonuclease H, *Sens. Actuators B Chem.*, 2020, **316**, 28072.

9 M. Irfan, P. S. Suprajaa, R. Praveen and B. M. Reddy, Microwave-assisted one-step synthesis of nanohydroxyapetite from fish bones and mussel shells, *Mater. Lett.*, 2021, **282**, 28685.

10 A. R. P. Puthukkara, S. T. Jose and D. S. Lal, Plant mediated synthesis of zero valent iron nanoparticles and its

application in water treatment, *J. Environ. Chem. Eng.*, 2021, **9**(1), 104569.

11 M. Nasrollahzadeh, M. Sajjadi and S. M. Sajadi, Biosynthesis of copper nanoparticles supported on manganese dioxide nanoparticles using Centella asiatica L. leaf extract for the efficient catalytic reduction of organic dyes and nitroarenes, *Chinese J. Catal.*, 2018, **39**, 109–117.

12 M. Bordbar, N. Negahdar and M. Nasrollahzadeh, Melissa Officinalis L. leaf extract assisted green synthesis of CuO/ZnO nanocomposite for the reduction of 4-nitrophenol and Rhodamine B, *Sep. Purif. Technol.*, 2018, **191**, 295–300.

13 J. K. Park, E. J. Rupa, M. H. Arif, L. F. Li, G. Anandapadmanaban, J. P. Kang, M. Kim, J. C. Ahn, R. Akter, D. C. Yang and S. C. Kang, Synthesis of zinc oxide nanoparticles from Gynostemma pentaphyllum extracts and assessment of photocatalytic properties through malachite green dye decolorization under UV illumination-A Green Approach, *Optik*, 2021, **239**, 166249.

14 N. Sarwar, U. B. Humayoun, M. Kumar, S. F. A. Zaidi, J. H. Yoo, N. Ali, D. I. Jeong, J. H. Lee and D. H. Yoon, Citric acid mediated green synthesis of copper nanoparticles using cinnamon bark extract and its multifaceted applications, *J. Clean. Prod.*, 2021, **292**, 125974.

15 M. Nasrollahzadeh, M. Sajjadi, J. Dadashi and H. Ghafuri, Pd-based nanoparticles: plant-assisted biosynthesis, characterization, mechanism, stability, catalytic and antimicrobial activities, *Adv. Colloid Interface Sci.*, 2020, **276**, 102103.

16 T. Parandhaman, M. D. Dey and S. K. Das, Biofabrication of supported metal nanoparticles: exploring the bioinspiration strategy to mitigate the environmental challenges, *Green Chem.*, 2019, **21**(20), 5469–5500.

17 A. L. Desa, N. H. H. Hairom, L. Y. Ng, C. Y. Ng, M. K. Ahmad and A. W. Mohammad, Industrial textile wastewater treatment via membrane photocatalytic reactor (MPR) in the presence of ZnO-PEG nanoparticles and tight ultrafiltration, *J. Water Process. Eng.*, 2019, **31**, 100872.

18 C. B. Ong, A. W. Mohammad and L. Y. Ng, Integrated adsorption-solar photocatalytic membrane reactor for degradation of hazardous Congo red using Fe-doped ZnO and Fe-doped ZnO/rGO nanocomposites, *Environ. Sci. Pollut. Res.*, 2019, **33**, 33856–33869.

19 N. K. Abdulla, S. I. Siddiqui, N. Tara, A. A. Hashmi and S. A. Chaudhry, Psidium guajava leave-based magnetic nanocomposite γ-Fe2O3@GL: a green technology for methylene blue removal from water, *J. Environ. Chem. Eng.*, 2019, **6**, 103423.

20 O. Üner, Hydrogen storage capacity and methylene blue adsorption performance of activated carbon produced from Arundo donax, *Mater. Chem. Phys.*, 2019, **237**, 121858.

21 A. Bhati, S. R. Anand, Gunture, A. K. Garg, P. Khare and S. K. Sonkar, Sunlight-induced photocatalytic degradation of pollutant dye by highly fuorescent red-emitting Mg-N-embedded carbon dots, *ACS Sustainable Chem. Eng.*, 2018, **6**, 9246–9256.

22 M. Shanmugam, A. Alsalme, A. Alghamdi and R. Jayavel, Enhanced photocatalytic performance of the graphene-V2O5 nanocomposite in the degradation of methylene blue dye under direct sunlight, *ACS Appl. Mater. Interfaces*, 2015, **7**, 14905–14911.

23 P. Khare, A. Singh, S. Verma, A. Bhati, A. K. Sonker, K. M. Tripathi and S. K. Sonkar, Sunlight-induced selective photocatalytic degradation of methylene blue in bacterial culture by pollutant soot derived nontoxic graphene nanosheets, *ACS Sustainable Chem. Eng.*, 2018, **6**, 579–589.

24 X. Li, R. Shen, S. Ma, X. Chen and J. Xie, Graphene-based heterojunction photocatalysts, *Appl. Surf. Sci.*, 2018, **430**, 53–107.

25 A. A. Shah, M. A. Bhatti, A. Tahira, A. D. Chandio, I. A. Channa, A. G. Sahito, E. Chalangar, M. Willander, O. Nurand and Z. H. Ibupoto, Facile synthesis of copper doped ZnO nanorods for the efficient photo degradation of methylene blue and methyl orange, *Ceram. Int.*, 2020, **46**, 9997–10005.

26 J. Wen, J. Xie, X. Chen and X. Li, A review on g-C3N4-based photocatalysts, *Appl. Surf. Sci.*, 2017, **391**, 72–123.

27 N. L. Stock, J. Peller, K. Vinodgopal and P. V. Kamat, Combinative sonolysis and photocatalysis for textile dye degradation, *Environ. Sci. Technol.*, 2000, **34**, 1747–1750.

28 B. C. M. Martindale, G. A. M. Hutton, C. A. Caputo and E. Reisner, Solar hydrogen production using carbon quantum dots and a molecular nickel catalyst, *J. Am. Chem. Soc.*, 2015, **137**, 6018–6025.

29 J. Gröttrup, F. Schütt, D. Smazna, O. Lupan, R. Adelung and Y. K. Mishra, Porous ceramics based on hybrid inorganic tetrapodal networks for efficient photocatalysis and water purification, *Ceram. Int.*, 2017, **43**, 14915–14922.

30 J. Pan, J. Liu, S. Zuo, U. A. Khan, Y. Yu and B. Li, Structure of Z-scheme CdS/CQDs/BiOCl heterojunction with enhanced photocatalytic activity for environmental pollutant elimination, *Appl. Surf. Sci.*, 2018, **444**, 177–186.

31 M. A. Bhatti, A. A. Shah, K. F. Almaani, A. Tahira, A. D. Chandio, M. Willander, O. Nur, A. Q. Mugheri, A. L. Bhatti, B. Waryani, A. Nafady and Z. A. Ibupoto, TiO2/ZnO Nanocomposite Material for Efficient Degradation of Methylene Blue, *J. Nanosci. Nanotechnol.*, 2021, **21**, 2511–2519.

32 X. Xu, R. Ray, Y. Gu, H. J. Ploehn, L. Gearheart, K. Raker and W. A. Scrivens, Electrophoretic Analysis and Purification of Fluorescent Single-Walled Carbon Nanotube Fragments, *J. Am. Chem. Soc.*, 2004, **40**, 12736–12737.

33 Y. Cheng, M. Bai, J. Su, C. Fang, H. Li, J. Chen and J. Jiao, Synthesis of fluorescent carbon quantum dots from aqua mesophase pitch and their photocatalytic degradation activity of organic dyes, *J. Mater. Sci. Technol.*, 2019, **8**, 1515–1522.

34 A. Yadav, L. Bai, Y. Yang, J. Liu, A. Kaushik, G. J. Cheng, L. Jiang, L. Chi and Z. Kang, Lasing behavior of surface functionalized carbon quantum dot/RhB composites, *Nanoscale*, 2017, **16**, 5049–5054.

35 P. Namdari, B. Negahdari and A. Eatemadi, Synthesis, properties and biomedical applications of carbonbased quantum dots: an updated review, *Biomed. Pharmacother.*, 2017, **87**, 209–222.

36 J. Di, J. Xia, Y. Ge, H. Li, H. Ji, H. Xu, Q. Zhang, H. Li and M. Li, Novel visible-light-driven CQDs/Bi2WO6 hybrid materials with enhanced photocatalytic activity toward organic pollutants degradation and mechanism insight, *Appl. Catal. B: Environ.*, 2015, **168–169**, 51–61.

37 X. Zhang, M. Jiang, N. Niu, Z. Chen, S. Li, S. Liu and J. Li, Natural-Product-Derived Carbon Dots: From Natural Products to Functional Materials, *ChemSusChem*, 2018, **1**, 11–24.

38 P. Miao, K. Han, Y. Tang, B. Wang, T. Lin and W. Cheng, Recent advances in carbon nanodots: synthesis, properties and biomedical applications, *Nanoscale*, 2015, **5**, 1586–1595.

39 S. Dey, A. Govindaraj, K. Biswas and C. N. R. Rao, Luminescence properties of boron and nitrogen doped graphene quantum dots prepared from arc-discharge-generated doped graphene samples, *Chem. Phys. Lett.*, 2014, **595–596**, 203–208.

40 L. Cao, X. Wang, M. J. Meziani, F. Lu, H. Wang, P. G. Luo, Y. Lin, B. A. Harruff, L. M. Veca, D. Murray and S. Y. Xie, Carbon Dots for Multiphoton Bioimaging, *J. Am. Chem. Soc.*, 2007, **37**, 11318–11319.

41 H. Li, Z. Kang, Y. Liu and S. T. Lee, Carbon nanodots: synthesis, properties and applications, *J. Mater. Chem.*, 2012, **22**(46), 24230–24253.

42 S. Sahu, B. Behera, T. K. Maiti and S. Mohapatra, Simple one-step synthesis of highly luminescent carbon dots from orange juice: application as excellent bio-imaging agents, *Chem. Commun.*, 2012, **70**, 8835–8837.

43 Z. Zhan, S. Zhao and M. Xue, Green preparation of fluorescent carbon dots from water chestnut and its application for multi-colour imaging in living cells, *Dig. J. Nanomater.*, 2017, **12**, 555–564.

44 A. Sachdev and P. Gopinath, Green synthesis of multi-functional carbon dots from coriander leaves and their potential application as anti-oxidants, sensors and bio-imaging, *Analyst*, 2015, **140**, 4260–4269.

45 A. Tyagi, K. M. Tripathi, N. Singh, S. Choudhary and R. K. Gupta, Green synthesis of carbon quantum dots from lemon peel waste: application in sensing and photo catalysis, *RSC Adv.*, 2016, **6**, 72423–72432.

46 N. R. Pries, C. M. W. Santos, R. R. Sousa, R. C. M. d Paule, P. L. R. Cunha and J. P. A. Feista, Novel and fast microwave-assisted synthesis of carbon quantum dots from cashew gum, *J. Braz. Chem. Soc.*, 2015, **26**, 1274–1282.

47 X. Yang, Y. Zhuo, S. Zhu, Y. Luo, Y. Feng and Y. Dou, Novel and green synthesis of high-fluorescent carbon dots originated from honey for sensing and imaging, *Biosens. Bioelectron.*, 2014, **60**, 292–298.

48 S. Sahu, B. Behara, T. K. Maiti and S. Mohapatra, Simple one-step synthesis of highly luminescent carbon dots from orange juice: application as excellent bioimaging agents, *Chem. Commun.*, 2012, **48**, 8835–8837.

49 A. Prasannan and T. Imae, One-pot synthesis of fluorescent carbon dots from orange waste peels, *Ind. Eng. Chem. Res.*, 2013, **52**, 15673–15678.

50 W. Liu, H. Diao, H. Chang, H. Wang, T. Li and W. Wei, Green Synthesis of carbon dots from rose-heart radish and application for Fe3+ detection and cell imaging, *Sens. Actuators B Chem.*, 2017, **241**, 190–198.

51 Q. Ye, F. Yan, Y. Luo, Y. Wang, X. Zhou and L. Chen, Formation of N, S-codoped fluorescent carbon dots from biomass and their application for the selective detection for the selective detection of mercury and iron ion, *Spectrochim. Acta, Part A*, 2017, **173**, 854–862.

52 D. L. D'souza, B. Deshmukh, B. R. Bhamore, K. A. Rawat, N. Lenka and S. K. Kailasa, Synthesis of fluorescent nitrogen-doped carbon dots from dried shrimps for cell imaging and boldine drug delivery system, *RSC Adv.*, 2016, **6**, 12169–12179.

53 V. Arul, T. N. J. I. Edison, Y. R. Lee and M. G. Sethuraman, Biological and catalytic applications of green synthesized fluorescent N-doped carbon dots using Hylocereus undatus, *J. Photochem. Photobiol. B, Biol.*, 2017, **168**, 142–148.

54 L. Wang and H. S. Zhou, Green synthesis of luminescent nitrogen-doped carbon vdots from milk and its imaging application, *Anal. Chem.*, 2014, **86**, 8902–8905.

55 V. N. Mehta, R. K. Singhaln and S. K. Kailasa, One step hydrothermal approach to fabricate caron dots from apple juice for imaging of mycobacterium and fungal cells, *Sens. Actuators B Chem.*, 2015, **213**, 434–443.

56 A. Somasundaram, V. Anjugam, J. Velu, S. Gandhi, S. Subramanian, K. Konda Ramasamy and V. Balasubramanian, Highly fluorescent carbon dots from Pseudostem of banana plant: applications as nanosensor and bio-imaging agents, *Sens. Actuators B Chem.*, 2017, **252**, 894–900.

57 A. Somasundaram, V. Anjugam, N. Sampathkumar, J. Shanmugapriya, S. Gandhi, S. Subramanian, M. Shanmugam and V. Balasubramanian, Pineapple peel-derived carbon dots: applications as sensor, molecular keypad lock, and memory device, *ACS Omega*, 2018, **3**, 12584–12592.

58 N. Gao, L. Huang, T. Li, J. Song, H. Hu, Y. Liu and S. Ramakrishna, Application of carbon dots in dye-sensitized solar cells: a review, *J. Appl. Polym. Sci.*, 2020, **137**, 1–11.

59 Y. Zhao, J. Duan, B. He, Z. Jiao and Q. Tang, Improved charge extraction with n-doped carbon quantum dots in dye-sensitized solar cells, *Electrochim. Acta*, 2018, **282**, 255–262.

60 B. Rezaei, N. Irannejad, A. A. Ensafi and N. Kazemifard, The impressive effect of eco-friendly carbon dots on improving the performance of dye-sensitized solar cells, *Sol. Energy*, 2019, **182**, 412–419.

61 J. Briscoe, A. Marinovic, M. Sevilla, S. Dunn and M. Titirici, Biomass-derived carbon quantum dot sensitizers for solid-state nanostructured solar cells, *Angew. Chem., Int. Ed.*, 2015, **54**, 4463–4468.

62 U. Abd Rani, L. Y. Ng, C. Y. Ng, E. Mahmoudi, Y. S. Ng and A. W. Mohammad, Sustainable production of nitrogen-doped carbon quantum dots for photocatalytic degradation of methylene blue and malachite green, *J. Water Process. Eng.*, 2021, **40**, 101816.

63 M. A. Bhatti, K. F. Almaani, A. A. Shah, A. Tahira, A. D. Chandio, A. Q. Mugheri and Z. A. Ibupoto, Low Temperature Aqueous Chemical Growth Method for the Doping of W into ZnO Nanostructures and Their Photocatalytic Role in the Degradation of Methylene Blue, *J. Cluster Sci.*, 2021, 1–12.

64 Y. Yang, J. Cui, M. Zheng, C. Hu, S. Tan, Y. Xiao, Q. Yang and Y. Liu, One-step synthesis of amino-functionalized fluorescent carbon nanoparticles by hydrothermal carbonization of chitosan, *Chem. Commun.*, 2012, **48**, 380–382.

65 H. Tetsuka, R. Asahi, A. Nagoya, K. Okamoto, I. Tajima, R. Ohta and A. Okamoto, Optically tunable amino-functionalized graphene quantum dots, *Adv. Mater.*, 2012, **24**, 5333–5338.

66 S. H. Jin, D. H. Kim, G. H. Jun, S. H. Hong and S. Jeon, Tuning the photoluminescence of graphene quantum dots through the charge transfer effect of functional groups, *ACS Nano*, 2013, **7**, 1239–1245.

67 S. Sugiarti and N. Darmawan, Synthesis of fluorescence carbon nanoparticles from ascorbic acid, *Indones. J. Chem.*, 2015, **15**, 141–145.

68 Z. Zhang, W. Sun and P. Wu, Highly photoluminescent carbon dots derived from egg white: facile and green synthesis, photoluminescence properties, and multiple applications, *ACS Sustainable Chem. Eng.*, 2015, **3**, 1412–1418.

69 G. Eda, Y. Y. Lin, C. Mattevi, H. Yamaguchi, H. A. Chen, I. S. Chen, C. W. Chen and M. Chhowalla, Blue photoluminescence from chemically derived graphene oxide, *Adv. Mater.*, 2010, **22**, 505–509.

70 D. Y. Pan, J. C. Zhang, Z. Li and M. H. Wu, Hydrothermal Route for Cutting Graphene Sheets into Blue-Luminescent Graphene Quantum Dots, *Adv. Mater.*, 2010, **22**, 734–738.

71 M. Zheng, Z. G. Xie, D. Qu, D. Li, P. Du, X. B. Jing and Z. C. Sun, On-Off-On Fluorescent Carbon Dot Nanosensor for Recognition of Chromium(VI) and Ascorbic Acid Based on the Inner Filter Effect, *ACS Appl. Mater. Interfaces*, 2013, **5**, 13242–13247.

72 W. J. Wang, X. Hai, Q. X. Mao, M. L. Chen and J. H. Wang, Polyhedral oligomeric silsesquioxane functionalized carbon dots for cell imaging, *ACS Appl. Mater. Interfaces*, 2015, **7**, 16609–16616.

73 T. Wang, A. Wang, R. Wang, Z. Liu, Y. Sun, G. Shan and Y. Liu, Carbon dots with molecular fluorescence and their application as a "turn-off" fluorescent probe for ferricyanide detection, *Sci. Rep.*, 2019, **9**, 1–9.

74 H. P. Jing, C. C. Wang, Y. W. Zhang, P. Wang and R. Li, Photocatalytic degradation of methylene blue in ZIF-8, *RSC Adv.*, 2014, **4**, 54454–54462.

75 U. G. Akpan and B. H. Hameed, Parameters affecting the photocatalytic degradation of dyes using TiO2-based photocatalysts: a review, *J. Hazard. Mater.*, 2009, **170**(2–3), 520–529.

76 L. L. F. Wen, J. Wang, L. Feng, C. G. Lv, C. G. Wang and D. F. Li, Structures, photoluminescence, and photocatalytic properties of six new metal-organic frameworks based on aromatic polycarboxylate acids and rigid imidazole-based synthons, *Cryst. Growth Des.*, 2009, **9**, 3581–3589.

77 M. N. Chong, B. Jin, C. W. K. Chow and C. Saint, Recent developments in photocatalytic water treatment technology: a review, *Water Res.*, 2010, **44**, 2997–3027.

78 J. Guo, F. Dong, S. Zhong, B. Zhu, W. Huang and S. Zhang, TiO2–hydroxyapatite composite as a new support of highly active and sintering-resistant gold nanocatalysts for catalytic oxidation of CO and photocatalytic degradation of methylene blue, *Catal. Lett.*, 2018, **148**, 359–373.

79 A. Singh Vig, A. Gupta and O. P. Pandey, Efficient photodegradation of methylene blue (MB) under solar radiation by ZrC nanoparticles, *Adv. Powder Technol.*, 2018, **29**, 2231–2242.

80 S. Mallakpour and M. Hatami, LDH-VB9-TiO2 and LDH-VB9-TiO2/crosslinked PVA nanocomposite prepared via facile and green technique and their photo-degradation application for methylene blue dye under ultraviolet illumination, *Appl. Clay Sci.*, 2018, **163**, 235–248.

81 H. R. Pouretedal and A. Kadkhodaie, Synthetic CeO2 nanoparticle catalysis of methylene blue photodegradation: kinetics and mechanism, *Chin. J. Catal.*, 2010, **31**, 1328–1334.

82 M. Jacob, R. Rajan, M. Aji, G. G. Kurup and A. Pugazhendhi, Bio-inspired ZnS quantum dots as efficient photo catalysts for the degradation of methylene blue in aqueous phase, *Ceram. Int.*, 2019, **45**, 4857–4862.

83 G. S. Sunil, K. M. Vilas, P. P. Sandip and H. S. Gunvant, Effect of doping parameters on photocatalytic degradation of methylene blue using Ag doped ZnO nanocatalyst, *SN Appl. Sci.*, 2020, **2**, 820.

84 B. Mondol, A. Sarker, A. M. Shareque, S. C. Dey, M. T. Islam, A. K. Das, S. M. Shamsuddin, M. A. I. Molla and M. Sarker, Preparation of Activated Carbon/TiO2 Nanohybrids for Photodegradation of Reactive Red-35 Dye Using Sunlight, *Photochem*, 2021, **1**, 54–56.

85 M. A. I. Molla, I. Tateishi, M. Furukawa, H. Katsumata, T. Suzuki and S. Kaneco, Evaluation of Reaction Mechanism for Photocatalytic Degradation of Dye with Self-Sensitized TiO2 under Visible Light Irradiation, *Open J. Inorg. Non-Met. Mater.*, 2017, **7**, 1–7.

86 A. J. Laghari, U. Aftab, A. Tahira, A. A. Shah, A. Gradone, M. Y. Solangi, A. H. Samo, M. kumar, M. I. Abro, M. W. Akhtar, R. Mazzaro, V. Morandi, A. M. Alotaibi, A. Nafady, A. I. Molina and Z. H. Ibupoto, MgO as promoter for electrocatalytic activities of Co3O4–MgO composite via abundant oxygen vacancies and Co2+ ions towards oxygen evolution reaction, *Int. J. Hydrog. Energy*, 2022, **04**, 169.

87 D. Hartanto, G. Yuhaneka, W. P. Utomo, A. I. Rozafia, Y. Kusumawati, W. Dahani and A. Iryani, *RSC Adv.*, 2022, **12**, 5665–5676.

88 Z. Zhu, P. Yang, X. Li, M. Luo, W. Zhang, M. Chen and X. Zhou, Green preparation of palm powder-derived carbon dots co-doped with sulfur/chlorine and their application in visible-light photocatalysis, *Spectrochim. Acta A Mol. Biomol. Spectrosc.*, 2020, **227**, 117659.

89 A. Aghamali, M. Khosravi, H. Hamishehkar, N. Modirshahla and M. A. Behnajady, Synthesis and characterization of high efficient photoluminescent sunlight driven photocatalyst of N-Carbon Quantum Dots, *J. Lumin.*, 2018, **201**, 265–274.

90 W. Wang, Y. Ni and Z. Xu, One-step uniformly hybrid carbon quantum dots with high-reactive TiO2 for photocatalytic application, *J. Alloys Compd.*, 2015, **622**, 303–308.

91 V. Ramar, S. Moothattu and K. Balasubramanian, Metal free, sunlight and white lightbased photocatalysis using carbon quantum dots from Citrus grandis: a green way to remove pollution, *Sol. Energy*, 2018, **169**, 120–127.

92 J. Zhang, X. Zhang, S. Dong, X. Zhou and S. Dong, N-doped carbon quantum dots/TiO2 hybrid composites with enhanced visible light driven photocatalytic activity toward dye wastewater degradation and mechanism insight, *J. Photochem. Photobiol. A*, 2016, **325**, 104–110.

93 M. Rahbar, M. Mehrzad, M. Behpour, S. Mohammadi-Aghdam and M. Ashrafi, S, N co-doped carbon quantum dots/TiO2 nanocomposite as highly efficient visible light photocatalyst, *Nanotechnology*, 2019, **30**, 505702.

94 Y. Hou, Q. Lu, H. Wang, H. Li, Y. Zhang and S. Zhang, One-pot electrochemical synthesis of carbon dots/TiO2 nanocomposites with excellent visible light photocatalytic activity, *Mater. Lett.*, 2016, **173**, 13–17.

95 Z. Zhang, T. Zheng, J. Xu, H. Zeng and N. Zhang, Carbon quantum dots/Bi2MoO6 composites with photocatalytic H2 evolution and near infrared activity, *J. Photochem. Photobiol. A*, 2017, **346**, 24–31.

96 Y. Cheng, M. Bai, J. Su, C. Fang, H. Li, J. Chen and J. Jiao, Synthesis of fluorescent carbon quantum dots from aqua mesophase pitch and their photocatalytic degradation activity of organic dyes, *J. Mater. Sci. Technol.*, 2019, **35**, 1515–1522.

97 M. Saikia, T. Das, N. Dihingia, X. Fan, L. F. Silva and B. K. Saikia, Formation of carbon quantum dots and graphene nanosheets from different abundant carbonaceous materials, *Diamond Relat. Mater.*, 2020, **106**, 107813.

98 U. R. R. P. Remli and A. A. Aziz, Photocatalytic degradation of methyl orange using Carbon Quantum Dots (CQDs) derived from watermelon rinds, *IOP Conf. Ser.: Mater. Sci. Eng.*, 2020, **736**, 042038.

99 T. T. V. Nu, N. H. T. Tran, P. L. Truong, B. T. Phan, M. N. T. Dinh, V. P. Dinh and V. Van Tran, Green synthesis of microalgae-based carbon dots for decoration of TiO2 nanoparticles in enhancement of organic dye photodegradation, *Environ. Res.*, 2022, **206**, 112631.

100 C. Wang, J. Xu, R. Zhang and W. Zhao, Facile and low-energy-consumption synthesis of dual-functional carbon dots from Cornus walteri leaves for detection of p-nitrophenol and photocatalytic degradation of dyes, *Colloids Surf., A*, 2022, 128351.